ACS Catalysis

Research Article

pubs.acs.org/acscatalysis

Toward Optimizing the Performance of Self-Regenerating Pt-Based Perovskite Catalysts

Ignace Jarrige,*[,†,⊥] Kenji Ishii,[†] Daiju Matsumura,[†] Yasuo Nishihata,[†] Masahiro Yoshida,[†,∥] Hirofumi Kishi,[‡,▽] Masashi Taniguchi,[§] Mari Uenishi,[§] Hirohisa Tanaka,[§] Hideaki Kasai,[‡] and Jun'ichiro Mizuki[†,∥]

[†]Japan Atomic Energy Agency, SPring-8, 1-1-1 Kouto, Sayo, Hyogo 679-5148, Japan

[‡]Department of Precision Science and Technology and Applied Physics, Osaka University, 2-1 Yamada-oka, Suita, Osaka 565-0871, Japan

[§]Daihatsu Motor Co., Ltd., Research and Development Division, 3000 Yamanoue, Ryuo, Gamo, Shiga 520-2593, Japan

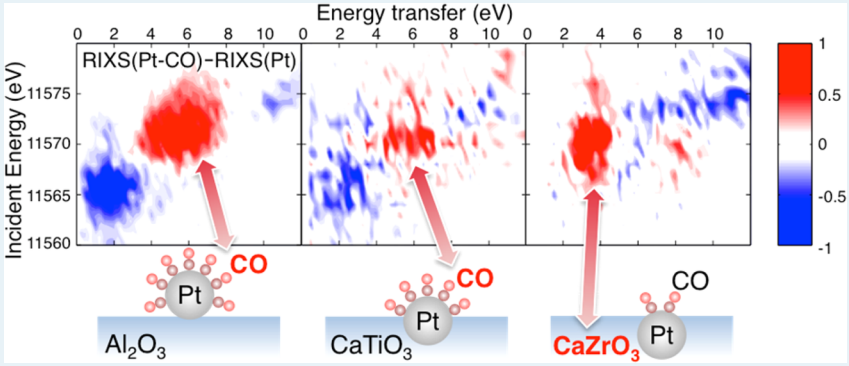

ABSTRACT: Self-regenerating automotive catalysts owe their remarkable performance to the repeated motion of the precious metal atoms in and out of the perovskite lattice under fluctuating oxidizing and reducing conditions, preventing coalescence of the metal nanoparticles. Here we use resonant inelastic X-ray scattering to characterize the occupied and unoccupied Pt 5d states in two self-regenerating Pt-perovskite catalysts, $CaTi_{0.95}Pt_{0.05}O_3$ and $CaZr_{0.95}Pt_{0.05}O_3$. Upon reduction, the element and symmetry-specific charge excitation spectra reveal a sizable hybridization between the Pt 5d and the Ti 3d or Zr 4d states at the interface between the nanoparticles and the perovskite, which involves the occupied states and is thus invisible in X-ray absorption spectra. A correlation is found between the strength of this d-band hybridization and the proportion of Pt nanoparticles that remain buried below the surface during reduction, indicating that the motion of the Pt atoms toward the surface is hindered by this hybridization specifically, rather than by the Pt−O bonding. These results provide direct evidence that the strength of the metal−metal d-band hybridization plays a pivotal role in determining the efficiency of self-regeneration in perovskite catalysts.

KEYWORDS: *platinum, perovskite, heterogeneous catalysis, nanoparticle, RIXS, XAS*

INTRODUCTION

Self-regeneration, a property of some perovskite catalysts to maintain a high activity during aging without requiring addition of excess precious metal, is a major discovery of modern-day automotive catalysis. The prospect of minimizing the amount of precious metal needed to satisfy stringent low-emission vehicle requirements has generated a large interest in the self-regeneration mechanism. A cornerstone of this research effort is the uncovering of the reversible motion of the precious-metal atoms into the perovskite lattice during oxidation, and out, forming nanoparticles on the surface, during reduction.[1] This motion was shown to prevent the agglomeration and growth of the metal particles during vehicle use. The proportion of precious metal cyclically moving in and out of the perovskite, called the self-regeneration ratio, has since then become the yardstick by which the self-regenerating performance is measured.[2] However, to date, little is known about the underlying physical mechanism of self-regeneration, and a unifying picture of self-regeneration and catalytic function is yet to emerge. Moreoever, there have been conflicting reports about the extent to which the precious atoms move out of the perovskite matrix during reduction.[1−4]

Although much of the focus in the literature has been on the structural aspect of the self-regeneration mechanism,[1,2,5] we here report a study of the electronic structure of two self-regenerating Pt-doped catalysts, $CaTi_{0.95}Pt_{0.05}O_3$ (CTPO) and $CaZr_{0.95}Pt_{0.05}O_3$ (CZPO), before and after CO adsorption. We

Received: October 17, 2014
Published: November 21, 2014

DOI: 10.1021/cs501608k
ACS Catal. 2015, 5, 1112−1118

employ resonant inelastic X-ray scattering (RIXS), an element and orbital-specific photon-in photon-out probe, to simultaneously characterize the interaction of the occupied and unoccupied Pt 5d bands with the metal d bands of the perovskite and with the O p states of CO. Upon reduction, we find a previously unobserved feature distinct from Pt−O (inside perovskite lattice) and Pt−Pt (nanoparticles on the surface) bondings, attributed to the hybridization between the Pt 5d and the Ti 3d or Zr 4d states at the interface between the Pt nanoparticles and the perovskite matrix. The relative intensity of this feature is found to be linked with the fraction of Pt nanoparticles remaining within the interior of the perovskite during reduction, uninvolved in gas-phase catalysis. These results indicate that the hybridization strength between metal d bands can be used to optimize the proportion of exposed precious-metal atoms during reduction in perovskite catalysts under different operating conditions.

MATERIALS AND METHODS

A. Sample Preparation. The preparation of both perovskite catalysts by the alkoxide method is described in detail elsewhere.[1,2] Pt(8 wt %)/γ-Al_2O_3 (PAO) was prepared by impregnating γ-Al_2O_3 with dilute aqueous $(NH_3)_2Pt(NO_2)_2$, dried, and calcined at 500 °C for 1 h in air. For all samples, 50 mg of powder was pressed into pellets of 7 mm in diameter. The PAO pellet was heated to 400 °C under a 100 cc/min flow of He at a rate of 20 K/min, reduced in H_2 at 400 °C for 10 min, and cooled to room temperature in the same H_2 atmosphere. The CZPO and CTPO pellets were heated to 800 °C under a 100 cc/min flow of He at a rate of 40 K/min, reduced in H_2 at 800 °C for 30 min, and cooled to room temperature in the same H_2 atmosphere. RIXS measurements in an H_2 atmosphere were performed just after this reductive treatment. Before the RIXS measurements in a CO atmosphere, the pellets were exposed to a CO (10%)/He atmosphere at room temperature after purging H_2 by He for 30 min. Before the RIXS measurements in an oxidizing atmosphere, the samples were heated in air during 5 min at 600 °C. The RIXS measurement on PtO_2 was performed on powder purchased from Wako Pure Chemical Industries (99% purity) pressed into a pellet.

B. X-ray Measurements. The RIXS and X-ray absorption spectroscopy (XAS) measurements were performed at the beamline BL11XU at SPring-8.[6] The undulator beam was monochromatized by a Si (111) double-crystal monochromator, and the energy bandwidth was further reduced using a 2-bounce channel-cut Si (400) monochromator. X-rays horizontally scattered by the sample were energy-analyzed using a spherically bent Si (755) analyzer. The total energy resolution of this setup estimated from the full width at half-maximum of the elastic line was 750 meV.

C. RIXS and the Fluorescence Processes. The RIXS and the fluorescence processes at the Pt L edge are illustrated in Figure 1. In RIXS, the absorption of a photon with an energy approaching the 2p binding energy excites an electron into localized empty 5d states above the Fermi level, E_F, in the intermediate state. An electron from the occupied 5d band then fills the core hole, and a photon is emitted in the final state. In this so-called Raman regime, the outgoing photon energy varies linearly with the incoming photon energy E_{inc}, thus the final state excitation energy, or energy transfer, is constant. The obtained spectrum can be seen as a convolution of the occupied and empty Pt 5d bands, also called joint density of states

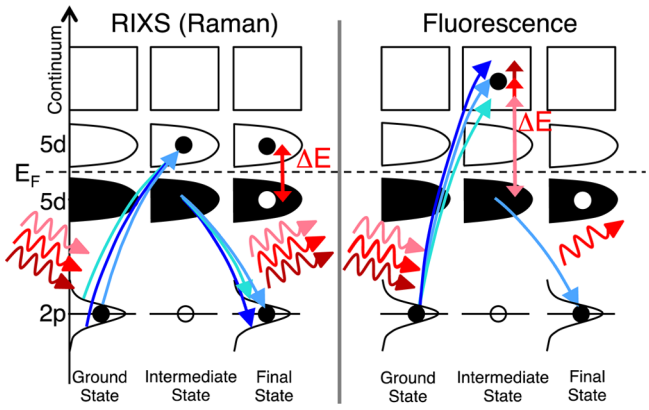

Figure 1. Schematic illustrations of the RIXS (Raman) and fluorescence processes. When varying E_{inc}, the charge excitation energy (ΔE) stays constant in Raman while the outgoing photon energy stays constant in fluorescence.

(JDOS). In the fluorescence regime, a 2p electron is ejected into delocalized states in the intermediate state, and a photon is emitted independently as a 5d electron fills the core hole in the final state. The emitted photon energy is constant and equal to the energy difference between the 2p and 5d levels. By exploiting the intensity ratio between the RIXS excitations and the fluorescence, one can assess the nature of the electronic states involved, localized (strong RIXS) or delocalized (strong fluorescence). This is illustrated when commenting on the RIXS planes in the section Results and Discussion.

D. Computational Details. The electronic structure calculations were performed by spin polarized density functional theory (DFT) using the VASP (Vienna ab initio simulation package) code.[7−10] The wave functions of the valence electrons were expanded in a basis set of plane waves with kinetic energy smaller than a cutoff of 400 eV. The interaction between ions and electrons was described using the projector augmented wave (PAW) method.[11,12] Reciprocal-space integration over the Brillouin zone was carried out on a 3 × 3 × 1 grid of Monkhorst−Pack k-points.[13] The approximation for the exchange-correlation function used is the generalized gradient approximation (GGA) based on the Perdew−Burke−Ernzerhof (PBE) functional.[14,15] Conjugate-gradient algorithm[16] was used to relax the ions into their ground state. Electric dipole correction layer in the vacuum area was used to cut the dipole interactions between the repeated image layer systems. Numerical convergence of the results was achieved with respect to the slab thickness, the kinetic energy cutoff, and the k-point mesh.

The Pt nanoparticles supported on Al_2O_3 and $CaZrO_3$ were modeled using a 2 × 2 supercell approach with tetrahedral Pt_4 cluster adsorbed on γ-Al_2O_3 (111) and $CaZrO_3$ (001) surfaces. The γ− Al_2O_3 slab was modeled using 32 Al and 48 O atoms and vacuum space of ∼25 Å, while the $CaZrO_3$ slab consists of 84 atoms (16 Ca, 16 Zr, 48 O, and 4 Pt) separated by ∼16 Å of vacuum. The Pt_4 cluster and the top 40 atoms of the slab were fully relaxed to obtain the stable adsorption structure of the cluster on a number of possible surface sites with different adsorption configurations.

RESULTS AND DISCUSSION

A. Comparison between Oxidizing and Reducing Atmospheres. Figure 2 shows the RIXS planes measured across the Pt L_3 edge for Pt nanoparticles supported on Al_2O_3

DOI: 10.1021/cs501608k
ACS Catal. 2015, 5, 1112−1118

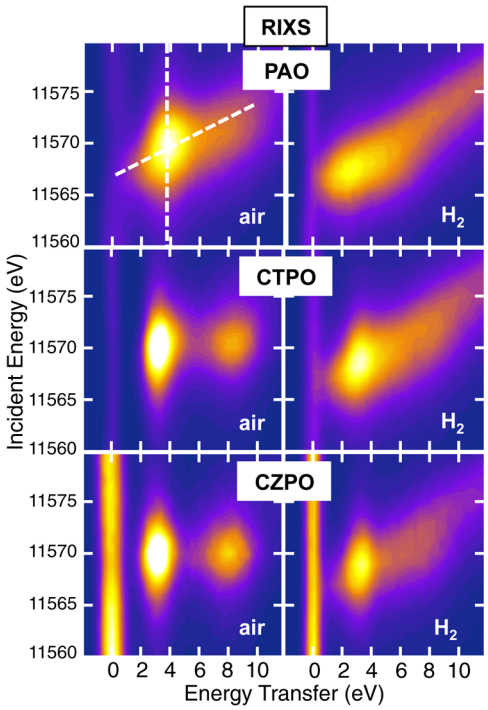

Figure 2. RIXS planes measured across the Pt-L_3 edge for PAO, CTPO, and CZPO, oxidized in air and after reduction in H_2.

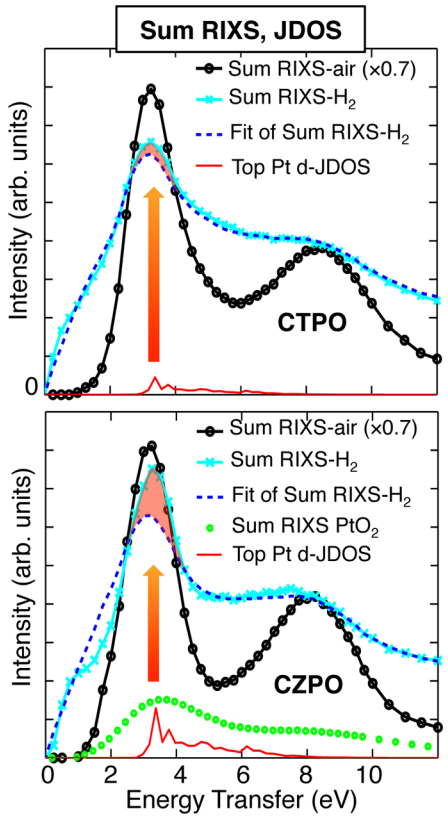

Figure 3. RIXS sum spectrum of the perovskites oxidized (sum RIXS-air), scaled in intensity by 0.7 for clarity, and of the perovskites reduced in H_2 (sum RIXS-H_2). A weighted sum of 20% of the sum RIXS-air spectra and 80% of PAO reduced in H_2 is used to fit the sum RIXS-H_2 spectra. The sum RIXS spectrum for PtO_2 and the Pt 5d JDOS of the top Pt site of a Pt_4 cluster supported on $CaZrO_3$ are also shown.

(PAO), CTPO, and CZPO after oxidation in air (left column) and reduction in H_2 (right column). The dashed lines in the contour plot of PAO highlight the opposite energy dispersions brought about by the RIXS and fluorescence processes. The streak of intensity along the E_{inc} axis corresponds to a RIXS excitation between the occupied and empty Pt 5d bands. Its spectral shape along the energy transfer is thus a measure of the Pt 5d JDOS. The fluorescence appears as a diagonal streak at constant emitted energy. The localized character of the Pt 5d states in the oxidized perovskites results in elongated vertical streaks, contrasting with the more pronounced fluorescence behavior in the RIXS plane of oxidized PAO. We also note that while the RIXS intensity stretches all the way down to 0 eV energy transfer for oxidized PAO, a gap between 0 and 2 eV energy transfer is open for the oxidized perovskites. These observations are in agreement with the fact that the perovskites are insulating, while PAO, even oxidized, retains a metallic character. Upon reduction, the fluorescence intensity strongly increases at the expense of the RIXS excitations for all three systems. This reflects the more delocalized nature of the electronic states in line with the expected metallization of Pt.

Armed with an understanding of the high sensitivity of RIXS to the degree of electronic localization, we analyze the RIXS intensity of CTPO and CZPO summed over the different intermediate states, which is obtained by summing the spectra of Figure 2 over E_{inc}. These so-called sum RIXS spectra are shown in Figure 3, where the elastic peaks have been subtracted by symmetrically folding their energy gain side at 0 eV. In the oxidized state (sum RIXS- air for CTPO and CZPO in Figure 3), Pt occupies the octahedrally coordinated B-site of the perovskite unit cell. Previous calculations of the Pt 5d DOS for the B-site showed two prominent structures at −2 and −7 eV in the occupied states, assigned to bonding and antibonding interactions with the O 2p states, and a single structure in the unoccupied states around 2 eV.[17] We thus assign the two RIXS peaks at 3 and 8 eV to transitions between the two structures in the occupied Pt 5d DOS and the structure in the empty Pt 5d DOS. Upon reduction, Pt atoms migrate toward the perovskite surface where metal particles form. The corresponding sum spectra (sum RIXS-H_2 for CTPO and CZPO in Figure 3) show an increase of their low-energy spectral weight, which signifies the filling of the characteristic band gap of the insulating perovskites. We also note the decrease of the 8 eV peak, entangled in a background stemming from fluorescence. In Figure 3, we performed a fit of the sum RIXS-H_2 spectra of CTPO and CZPO using two reference sum RIXS spectra each, PAO reduced in H_2 for the contribution from the metal particles and oxidized CTPO or CZPO for the contribution from the perovskite B-site, in the 80/20 ratio. The proportion of oxidized perovskite used in the weighted sum, 20%, was adjusted to match the height of the 8 eV peak characteristic of the B-site. An important result of this study is that the fit does not work well below 4 eV energy transfer, especially for CZPO. This discrepancy is highlighted by the red shadowed areas in Figure 3, where the fits are seen to generate too much spectral weight below 2.5 eV, and not enough in the 2.5−4 eV range. We suggest that the inability to properly fit the sum RIXS-H_2 spectra with only two contributions, metal particles on the surface and B-site, indicates the existence of an additional bonding interaction associated with the migration of Pt out of the perovskite lattice.

DOI: 10.1021/cs501608k
ACS Catal. 2015, 5, 1112−1118

We now discuss this additional bonding interaction. Because the perovskites release oxygen during reduction one could make the hypothesis that the nanoparticles contain a fraction of insulating Pt oxide, contributing to the spectral weight only above 2.5 eV and thereby offsetting the discrepancy between the sum RIXS-H_2 spectra and the fits in Figure 3. However, the spectral weight in the sum RIXS spectrum of bulk PtO_2 is seen to extend down to 1 eV in Figure 3, in agreement with the calculated gap of 1.25 eV.[18]

Including the spectrum of PtO_2 in the fit would thus add further spectral weight below 2.5 eV, implying that the formation of Pt oxide can be ruled out. A wider band gap was recently suggested to form through the Pt 5d − Zr 4d hybridization at the interface between Pt particles and the surface of $CaZrO_3$, based on DOS calculations for a Pt_4 cluster supported on $CaZrO_3$.[19] The DOS projected on one of the Pt sites in the bottom plane of the tetrahedral cluster, directly bonded to $CaZrO_3$, showed two features around −2 and −7 eV in the occupied states.[19] These DOS are strongly reminiscent of the DOS of Pt in the B-site, which also showed two features at −2 and −7 eV, as mentioned above.[17] Their contribution to the RIXS spectra should thus be indistinguishable from the B-site Pt, and can accordingly not explain the poor agreement with the fits. Here, using similar first-principle calculations, we projected the DOS on the top Pt atom of the Pt_4 cluster. The as-obtained DOS of the top Pt site of the Pt_4 cluster, which we refer to as top Pt-d DOS in the remainder of this paper, are shown in the bottom panel of Figure 4 along with an illustration of the cluster. Although the peak ascribed to the bonding interaction with O 2p at −7 eV has vanished, the large gap arising from the hybridization with the Zr 4d states in $CaZrO_3$ is found to persist. This shows that the Pt 5d − Zr 4d hybridization is effective beyond the first layer of Pt atoms in direct contact with the support, which can be attributed to the extended character of both orbitals involved. As shown in Figure 4, the opening of the gap in the top Pt-d DOS is brought about by the overlap with the occupied and unoccupied Zr d states, which are themselves separated by a large band gap. This gap is known to be 4.1 eV in bulk $CaZrO_3$.[20] It is therefore a combination of a strong hybridization between the d bands of Pt in the Pt_4 cluster and Zr in the $CaZrO_3$ substrate and the band gap originally present in bulk $CaZrO_3$[20] which results in the formation of a large band gap in the top Pt-d DOS. In contrast, in the case of PAO, the fact that the Pt atoms retain their metallic character upon adsorption on Al_2O_3 was ascribed to the weaker hybridization between the Pt and the Al electronic states.[19] This weak interfacial hybridization in PAO is further substantiated by the similarity between the sum spectra of reduced PAO and bulk Pt metal as seen in the left panel of Figure 5b.

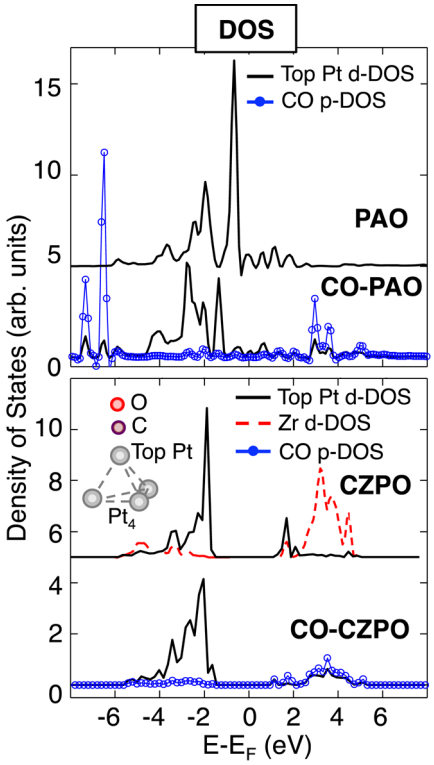

Figure 4. 5d DOS of the top Pt site of a Pt_4 cluster supported on an Al_2O_3 substrate (top panel) and of a Pt_4 cluster supported on a $CaZrO_3$ substrate (bottom panel). The DOS are shown both for the bare Pt clusters (PAO, CZPO) and for the Pt clusters with CO adsorbed (CO-PAO, CO-CZPO). The DOS are plotted as a function of $E - E_F$. The CO p and Zr d DOS are also shown.

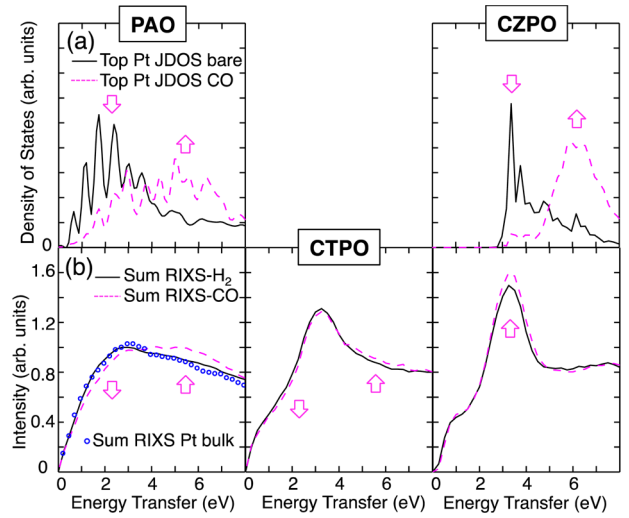

Figure 5. (a) Pt 5d JDOS obtained from the DOS in Figure 4 for PAO and CZPO. The arrows indicate the variations of intensity upon CO adsorption. (b) RIXS sum spectra of PAO, CTPO, and CZPO after reduction in H_2 and in CO. The spectrum of bulk platinum metal is also shown in the PAO inset.

The 5d JDOS of the top Pt site of the Pt_4 cluster, obtained by convoluting the occupied and unoccupied top Pt d-DOS from Figure 4, are shown in Figure 3. They are scaled in intensity to match the red shadowed areas of CTPO and CZPO. The close correspondence between the lineshapes of the peak formed by the JDOS and the red shadowed patterns seems to indicate that the contribution from the top Pt site of the Pt_4 cluster, which lacked in the fits of Figure 3, is at the origin of the disagreement between the sum spectra and the fits. This result confirms the occurrence of a substantial interfacial hybridization between the Pt 5d and Zr 4d orbitals in reduced CZPO, and of a similar, albeit weaker, Pt 5d−Ti 3d interfacial hybridization in reduced CTPO. One may wonder if this d-band hybridization could actually reveal the formation of Pt−Zr and Pt−Ti metallic alloys. Such alloys, because metallic, should however not yield a band gap. Their formation can therefore be discarded.

DOI: 10.1021/cs501608k
ACS Catal. 2015, 5, 1112−1118

We briefly comment on the fact that the d-band hybridization disclosed in this study affects the occupied DOS, as the unoccupied DOS are largely similar between the top site of the Pt_4 cluster on $CaZrO_3$ (Figure 4) and the perovskite B-site,[17] both showing a single peak around 2 eV. This suggests that XAS, which probes the unoccupied DOS, should be insensitive to this hybridization. In Figure 6, the XAS spectra measured at

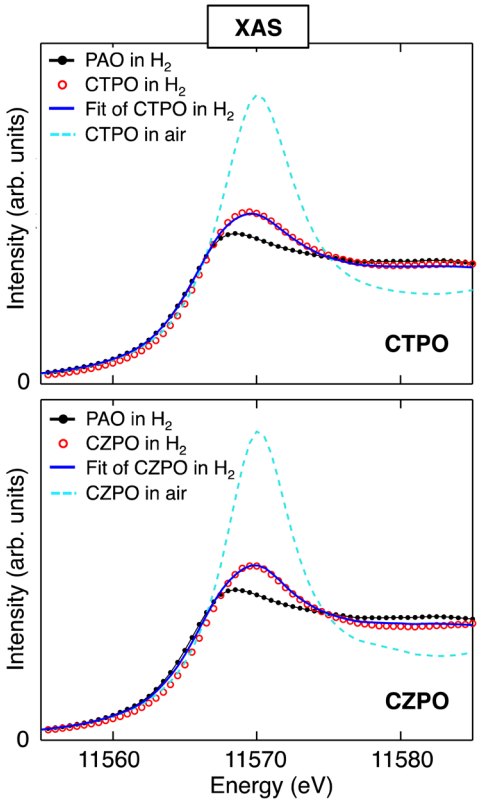

Figure 6. Pt-L_3 XAS spectra measured on PAO reduced in H_2 (both panels), CTPO reduced in H_2 and oxidized in air (top panel), CZPO reduced in H_2 and oxidized in air (bottom panel). The spectra of the perovskites in H_2 are satisfactorily fitted with a weighted sum of the perovskites in air and PAO in H_2.

the Pt-L_3 edge on CZPO and CTPO upon reduction are fitted with a weighted sum of PAO in H_2 and, respectively, CZPO and CTPO in their oxidized state. These fits are analogous to those in Figure 3 for the RIXS sum spectra. The weighted sums are $0.8 \times [\text{PAO in } H_2] + 0.2 \times [\text{CZPO in air}]$ for CZPO in H_2, and $0.83 \times [\text{PAO in } H_2] + 0.17 \times [\text{CTPO in air}]$ for CTPO in H_2. The fits are found to be successful, which shows that Pt-L_3 XAS, because probing the unoccupied Pt 5d states, can only detect two environments for the Pt atoms in the reduced perovskites, which are the metal nanoparticles on the surface and the B-site in the perovskite lattice. The technique is insensitive to the interfacial hybridization between the Pt 5d and Ti 3d or Zr 4d states. This stresses the importance to characterize both occupied and unoccupied states to understand the motion of the precious metal atoms in the self-regenerative catalysts.

B. Adsorption of CO. We now discuss the changes in the electronic structure of the Pt nanoparticles upon CO adsorption. The DOS of the top Pt atom in a Pt_4 cluster supported on Al_2O_3 and $CaZrO_3$ with CO adsorbed are shown in Figure 4, where they are, respectively, labeled CO-PAO and CO-CZPO. CO is adsorbed in the atop configuration, which we found to be energetically favorable. Upon hybridization with the O p states of CO, one observes that the Pt d states, at the exception of the occupied states of CZPO, are shifted away from the Fermi level. The Pt d JDOS for PAO and CZPO bare and after CO adsorption, obtained by convoluting the occupied and unoccupied Pt d DOS from Figure 4, are shown in Figure 5a. For both systems, the hybridization with the O p states of CO is found to result in a shift of the Pt d JDOS toward higher energies. In Figure 5b, the RIXS sum spectra are shown for all three systems (PAO, CTPO, CZPO) after thermal treatment in H_2 and after CO adsorption, which can be respectively compared with the JDOS bare and after CO adsorption of Figure 5a. Upon CO adsorption, the RIXS spectral weight of both PAO and CTPO is seen to increase around 6 eV and decrease around 2 eV, which is consistent with the shift toward higher energies in the JDOS of PAO. On the other hand, the RIXS sum spectrum of CZPO only shows an increase of its main peak around 3 eV, which is at odds with the shift found in the JDOS of CZPO. This discrepancy is addressed in detail in the next paragraph. We note that the overall amplitude of the adsorbate dependence of our RIXS data is weaker than in a previous RIXS study on PAO,[21] which we ascribe to the fact that our measurements were not performed under a constant flow, but in a sealed atmosphere of CO.

More information can be extracted from the RIXS data by looking at the contour plot of the difference between the RIXS planes measured before and after CO adsorption, shown in Figure 7b for all three systems. The purpose of these contour plots is to isolate and highlight the spectral weight transfer induced by the hybridization between Pt d and the O p states of CO. This intensity transfer occurs from the areas colored in blue toward those colored in red in the three panels of Figure 7b. Together with these contour plots, the intensity difference between before and after CO adsorption is shown for the corresponding RIXS sum spectra, corresponding to the RIXS plane intensity summed along the incident energy axis, and the calculated JDOS, in the three panels of Figure 7a. We note that the amplitude of the changes in the RIXS data upon CO adsorption is expected to scale with the proportion of Pt atoms located on the surface during reduction. In order to enable a semiquantitative comparison between the data from the different systems, the intensity is thus normalized to this proportion for all three systems.

Two important findings can be drawn from these plots. First, comparing Figure 7a,b for PAO and CTPO, one sees that CO adsorption results in spectral weight transfers between the same areas of the RIXS plane for both systems, although the transfer is weaker for CTPO. The respective energy transfers of the dip (~2 eV) and the peak (~6 eV) in the RIXS sum spectra of both systems also agree well with those in the JDOS of PAO (see Figure 7a). These observations show that CO is also adsorbed in the top configuration in CTPO, and while the weaker spectral weight transfer points to a lower adsorption capacity than PAO, it does provide evidence for a cyclical motion of Pt in CTPO that involves surface dispersion. This result contrasts with a recent study using transmission electron microscopy which questioned the cyclical motion of the precious metal in CTPO.[4] The second finding is that the changes in the RIXS signal of CZPO after changing the atmosphere to CO differ markedly from the other two systems, and disagree with the JDOS of CZPO. Strikingly, the two peaks at 3 and 8 eV, characteristic of B-site bonding, gain strength (see red areas in

DOI: 10.1021/cs501608k
ACS Catal. 2015, 5, 1112−1118

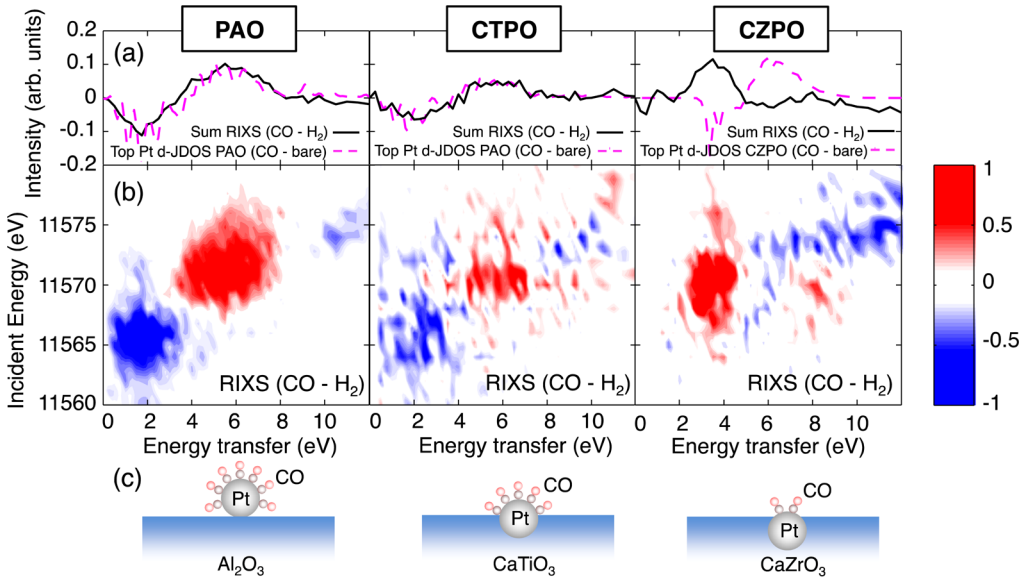

Figure 7. (a) Difference between the RIXS sum spectra of PAO, CTPO, and CZPO after reduction in CO and after reduction in H_2 (sum RIXS (CO − H_2)), superimposed with the difference between the 5d JDOS of the top Pt site after CO adsorption and bare. (b) Contour plot of the difference between the RIXS planes measured after CO adsorption and after reduction in H_2 for PAO, CTPO, and CZPO. (c) Illustration of the stronger metal−support interaction and the decreasing CO adsorption capacity along the PAO−CTPO−CZPO sequence.

Figure 7b), implying that Pt partially sinks into the support. It has been shown that during a reductive treatment of Pt nanoparticles in H_2, a fraction of the chemisorbed H atoms moves to the interface between the nanoparticles and the support.[22] Here, we speculate that changing the atmosphere to CO leads to the desorption of these H atoms. The Pt atoms are then left in direct contact with the support and, according to our data, are prone to sink into it when the metal−support interaction is strong as in CZPO. The fact that a similar increase of the 3 and 8 eV peaks does not occur for CTPO points to a weaker metal−support interaction.

Taken together, the RIXS data unveil concomitant trends of increased metal−support interaction and decreased CO adsorption capacity along the PAO-CTPO-CZPO sequence. From this inverse relationship, we here suggest that the contribution from the interfacial hybridized d states in the RIXS spectra of CTPO and CZPO originates from a fraction of Pt nanoparticles partly or entirely buried under the perovskite surface during reduction. A larger fraction of buried particles results in a larger interfacial area with the support, thus a stronger d-band hybridization between Pt and Ti or Pt and Zr, and also less interaction with CO. This reasoning is illustrated in Figure 7c. The strength of the interfacial d-band hybridization in the perovskite catalysts is thus a measure of the strength of the metal−support interaction. Because a larger fraction of nanoparticles retained below the perovskite surface during reduction implies a lower self-regeneration ratio, our results show that this d-band hybridization plays a key role in determining the self-regenerating ability of the perovskite catalysts.

We now address the difference in strength of d-band hybridization between CTPO and CZPO. On the one hand, the Zr 4d orbitals have a greater radial expansion than Ti 3d, which favors a larger overlap with the Pt 5d orbitals. On the other hand, interatomic distances are longer in CZPO, which hints at weaker bonds compared with CTPO. Our results show that the larger radial component of the Zr 4d orbitals is here the dominant factor and results in a larger overlap with the Pt 5d orbitals in CZPO than the Ti 3d orbitals in CTPO. Further, the metal-O bonds are longer in CZPO, and therefore, they are likely weaker than in CTPO.[23] This gives further credence to the idea that it is the stronger Pt−Zr d-band hybridization in CZPO compared with the Pt−Ti d-band hybridization in CTPO, which is at the source of the lower self-regeneration ability of CZPO, and not a difference in the Pt−O bond strength between the two systems. Our results can explain why a higher self-regeneration ratio was systematically achieved with titanates compared to zirconates in previously studied perovskite catalysts.[2] More generally, they can serve as a guide to optimize the surface redispersion of the precious metal atoms in self-regenerating catalysts via controlling the hybridization strength between the d bands of the precious metal and the transition metal in the perovskite. This optimization directly depends on the catalyst operating conditions. For severe conditions such as very high exhaust temperatures a strong d-band hybridization will be critical to limit the coarsening of the Pt particles. On the other hand, perovskite catalysts with a weaker d-band hybridization can become viable under relatively mild operating conditions and thus result in a larger catalytic surface area.

CONCLUSION

In conclusion, using RIXS, we have uncovered a sizable hybridization between d bands at the interface between Pt nanoparticles and the perovskite support in self-regenerating catalysts during reduction. The high sensitivity of RIXS to the interaction of the precious metal with both the support and the adsorbate enables us to perform the first comprehensive description of the four bonding environments of the precious metal in these complex systems: the B-sites in the perovskite lattice, the interface between the nanoparticles and the support, the metallic nanoparticles, and the adsorption sites at the surface of the nanoparticles. The strength of the d-band hybridization at the metal−support interface is related to the proportion of nanoparticles buried near the support surface during reduction, unavailable for catalytic activity. Migration of

DOI: 10.1021/cs501608k
ACS Catal. 2015, 5, 1112−1118

the Pt atoms toward the surface during reduction is thus hampered by this d-band hybridization, rather than by the Pt−O bonding in the perovskite lattice. This result marks a significant step forward in the understanding of the cyclical motion of the precious atoms in self-regenerating catalysts. It also suggests that the d-band hybridization between the precious atoms and the perovskite lattice can be used as a key tuning parameter in the design of self-regenerating catalysts to optimize their performance depending on their operating conditions. Finally, this d-band hybridization only affects the occupied states and thus cannot be detected by XAS, which highlights the potential of RIXS as a stand-alone technique for in situ characterization of the occupied and unoccupied electronic structure of catalysts.

AUTHOR INFORMATION

Corresponding Author

*E-mail: jarrige@bnl.gov.

Present Addresses

[⊥](for I.J.) Photon Sciences Directorate, Brookhaven National Laboratory, Upton, New York 11973, United States

[∥](For M.Y. and J.M.) School of Science and Technology, Kwansei Gakuin University, Sanda, Hyogo 669-1337, Japan

[∇](For H.K.) Daihatsu Motor Co., Ltd., Research and Development Division, 3000 Yamanoue, Ryuo, Gamo, Shiga 520-2593 Japan

Author Contributions

All authors have given approval to the final version of the manuscript.

Notes

The authors declare no competing financial interest.

ACKNOWLEDGMENTS

This work was supported by the Elements Science and Technology Project. The synchrotron radiation experiments were performed at the BL11XU of SPring-8 with the approval of the Japan Synchrotron Radiation Research Institute (JASRI) (Proposal Nos. 2011B3502, 2010B3502, 2010A3502, and 2009B3502).

REFERENCES

(1) Nishihata, Y.; Mizuki, J.; Akao, T.; Tanaka, H.; Uenishi, M.; Kimura, M.; Okamoto, T.; Hamada, N. *Nature* **2002**, *418*, 164−167.

(2) Tanaka, H.; Taniguchi, M.; Uenishi, M.; Kajita, N.; Tan, I.; Nishihata, Y.; Mizuki, J.; Narita, K.; Kimura, M.; Kaneko, K. *Angew. Chem., Int. Ed.* **2006**, *45*, 5998−6002.

(3) Katz, M. B.; Graham, G. W.; Duan, Y.; Liu, H.; Adamo, C.; Schlom, D. G.; Pan, X. *J. Am. Chem. Soc.* **2011**, *133*, 18090−18093.

(4) Katz, M. B.; Zhang, S.; Duan, Y.; Wang, H.; Fang, M.; Zhang, K.; Li, B.; Graham, G. W.; Pan, X. *J. Catal.* **2012**, *293*, 145−148.

(5) Hamada, I.; Uozomi, A.; Morikawa, Y.; Yanase, A.; Katayama-Yoshida, H. *J. Am. Chem. Soc.* **2011**, *133*, 18506−18509.

(6) Ishii, K.; Jarrige, I.; Yoshida, M.; Ikeuchi, K.; Inami, T.; Murakami, Y.; Mizuki, J. *J. Elec. Spec. Rel. Phen.* **2013**, *188*, 127−132.

(7) Kresse, G.; Furthmuller, J. *Comput. Mater. Sci.* **1996**, *6*, 15−50.

(8) Kresse, G.; Furthmuller, J. *Phys. Rev. B* **1996**, *54*, 11169−11186.

(9) Kresse, G.; Hafner, J. *Phys. Rev. B* **1993**, *47*, 558−561.

(10) Kresse, G.; Hafner, J. *Phys. Rev. B* **1994**, *49*, 14251−14269.

(11) Blöchl, P. E. *Phys. Rev. B* **1994**, *50*, 17953−17979.

(12) Kresse, G.; Joubert, J. *Phys. Rev. B* **1999**, *59*, 1758−1775.

(13) Monkhorst, H. J.; Pack, J. D. *Phys. Rev. B* **1976**, *13*, 5188−5192.

(14) Perdew, J. P.; Burke, K.; Ernzerhof, M. *Phys. Rev. Lett.* **1996**, *77*, 3865−3868.

(15) Perdew, J. P.; Burke, K.; Ernzerhof, M. *Phys. Rev. Lett.* **1997**, *78*, 1396−1396.

(16) Štich, I.; Car, R.; Parrinello, M.; Baroni, S. *Phys. Rev. B* **1989**, *39*, 4997−5004.

(17) Matar, S. F.; Demazeau, G.; Largeteau, A. *Chem. Phys.* **2008**, *352*, 92−96.

(18) Yang, Y.; Sugino, O.; Ohno, T. *AIP Advances* **2012**, *2*, 022172.1−022172.6.

(19) Arevalo, R. L.; Kishi, H.; Padama, A. A. B.; Moreno, J. L. V.; Kasai, H. *J. Phys.: Condens. Matter* **2013**, *25*, 222001.1−222001.4.

(20) Stoch, P.; Szczerba, J.; Lis, J.; Madej, D.; Pędzich, Z. *J. Europ. Cer. Soc.* **2012**, *32*, 665−670.

(21) Glatzel, P.; Singh, J.; Kvashnina, K. O.; van Bokhoven, J. A. *J. Am. Chem. Soc.* **2010**, *132*, 2555−2557.

(22) Vaarkamp, M.; Miller, J. T.; Modica, F. S.; Koningsberger, D. C. *J. Catal.* **1996**, *163*, 294−305.

(23) Koopmans, H. J. A.; van de Velde, G. M. H.; Gellings, P. J. *Acta Cryst. C* **1983**, *39*, 1323−1325.

DOI: 10.1021/cs501608k
ACS Catal. 2015, 5, 1112−1118